ELSEVIER

Journal of Alloys and Compounds 257 (1997) 36–45

Journal of ALLOYS AND COMPOUNDS

Crystal structure and magnetic ordering in $ErFe_6Ge_6$ studied by X-ray, neutron diffraction and magnetic measurements

O. Oleksyn[1,a], P. Schobinger-Papamantellos[a,*], J. Rodríguez-Carvajal[b], E. Brück[c], K.H.J. Buschow[c]

[a]*Laboratorium für Kristallographie, ETHZ, CH-8092 Zürich, Switzerland*

[b]*Laboratoire Léon Brillouin (CEA_CNRS), Centre d'Etudes de Saclay, 91191, Gif-sur-Yvette, France*

[c]*Van der Waals-Zeeman Institute, University of Amsterdam, 1018 XE Amsterdam, The Netherlands*

Received 5 December 1996

Abstract

The crystal structure and magnetic ordering of $ErFe_6Ge_6$ were studied by means of X-ray and neutron powder diffraction and on a single crystal. Our results suggest that $ErFe_6Ge_6$, when annealed after casting, adopts a crystal structure intermediate between the perfectly ordered $HoFe_6Sn_6$ structure type, and the disordered structure of the YCo_6Ge_6 type. The 293 K (high resolution) and the 4.5 K neutron data show that the antiferromagnetic reflections can be explained by a $2\times c$ cell enlargement of the YCo_6Ge_6-type unit cell. The collinear antiferromagnetic magnetic structure is composed of ferromagnetic Fe-sheets coupled antiferromagnetically along the c_h-axis. The Er moments become ordered only below 3 K. This ordering is ferromagnetic with the Er-moments directed along the a_h-axis. The fact that the ferromagnetic and the antiferromagnetic ordering types are described by two different magnetic space groups indicates the presence of two order parameters, which explains the independent behaviour of the Fe and Er sublattices. © 1997 Elsevier Science S.A.

Keywords: Rare earth iron germanide; Neutron diffraction; Magnetisation; Crystal structure; Magnetic structure

1. Introduction

The crystal structures and magnetic properties of RM_6Ge_6 phases (R—rare-earth, M—Cr, Mn, Fe) exhibit a great variety of behaviours. Venturini et al. [1] reported that the $ErFe_6Ge_6$ compound, when annealed at $T_{an}=1173$ K, crystallizes in the $HoFe_6Sn_6$ structure [2] (*Immm*, $a=8.103(2)$, $b=26.52(3)$, $c=5.108(3)$ Å). Thermomagnetic studies performed between 90–900 K showed that the Fe-sublattice is ordered antiferromagnetically ($T_N=470$ K). No evidence of magnetic ordering of the rare-earth sublattice was seen in this temperature range. Wang et al. [3] reported that the structure of $ErFe_6Ge_6$ is of the YCo_6Ge_6 type (*P6/mmm*, $a=5.107(2)$, $c=4.045(3)$ Å, $T_{an}=1173$ K) and that the Néel temperature of $ErFe_6Ge_6$, as determined by Mössbauer spectroscopy and differential scanning calorimetry, is slightly higher than that reported by Venturini et al. [1].

While the present study was being carried out, Ryan and Cadogan [4] published magnetic and Mössbauer data on the high temperature modification of the RFe_6Ge_6 compounds (as described by Venturini et al. [1]) and reported that the R moments give rise to ferromagnetic ordering at temperatures below 30 K, proceeding independently of the magnetic ordering of the Fe sublattice. For the R=Er compound they report an ordering temperature of 3 K. In the present investigation we studied the crystal structure of $ErFe_6Ge_6$ compound by X-ray and high resolution neutron powder diffraction at 293 K. The low-temperature magnetic ordering was studied by magnetic measurements made on single crystal and by neutron powder diffraction.

2. Experimental details

The $ErFe_6Ge_6$ powder sample used for neutron diffraction was prepared by arc melting from starting materials of at least 99.9% purity and annealed at 800 °C for 4 weeks in an evacuated quartz tube. The X-ray diffraction pattern was obtained on Sintex powder diffractometer (Cu K_α-radiation, step scanning mode, 0.02° step increment, 15–140° 2θ range). Neutron diffraction experiments were carried out at the facilities of the Orphée reactor (LLB-Saclay). The 293 K data were collected with the 2-axes

*Corresponding author.

[1]On leave from Institute of Inorganic Chemistry, Lviv State University, Lviv, Ukraine.

PII S0925-8388(96)03125-8

high resolution instrument 3T2 (20 detectors, λ=1.227 Å with a 0.05° step increment in 2θ in the 2θ range 2–155°). The data between 1.5–4.5 K were collected on the G4.1 diffractometer (800 cells multidetector, λ=2.426 Å with a 0.1° step increment in 2θ in the 2θ 4–83.9° range). For data evaluation the programs FULLPROF [5] and XTAL3.4 [6] were used.

A single crystal with dimensions 0.5×0.4×0.17 mm^3 was selected from the fragments of an ingot obtained after quenching from the liquid state to room temperature. This single crystal was examined by Laue and precision photographs and the field dependence of its magnetisation was studied on a SQUID magnetometer at various temperatures in the cryogenic range.

3. Crystal structure studied by X-ray diffraction

The powder sample used for neutron diffraction was first examined by X-ray diffraction (see Fig. 1). The pattern comprises Bragg reflections of the hexagonal YCo_6Ge_6 structure type (*P6/mmm*, a_h=5.10638(8), c_h=4.04995(7) Å, indicated as model I in the following). The refinement based on model I led to rather low reliability factors (Table 1a, Fig. 2a) showing that the Er and the Ge1-atoms partly (50%) occupy the 1(a) position at (0 0 0) and the 2(e) position at (0 0 z), respectively. This result confirms the findings of Wang et al. [3]. However, it does not explain the observation of several low-intensity reflections that may indicate a deviation from this model.

In fact, apart from the dominant reflections of the YCo_6Ge_6 structure type we observed several weak satellites (indicated by arrows in Fig. 1), although these latter were somewhat obscured by the presence of a wavy background.

The satellites were indexed on the basis of the YCo_6Ge_6 type unit cell $(a, c)_h$ in the orthohexagonal setting $(c, a\sqrt{3}, a)_h$ with the wave vector $\mathbf{q}=1/2a_o^*+1/3b_o^*$. The position of the satellites is in good agreement with the superstructure unit cell (*Immm*, 2*c*, $3a\sqrt{3}$, $a)_h$ proposed by Venturini et al. [1] (henceforth indicated as model II, Fig. 2b). The refinement based on model II led to higher reliability factors (R_n=26.0, R_{wp}=39.9, R_{exp}=6.39%, χ^2=39.0), as expected due to the low signal/noise ratio of the few observed superstructure reflections. The calculated intensities of the satellites were essentially higher than the observed ones. This indicates that the long-range ordered distribution of Er-atoms and of Ge_2-pairs in the hexagonal channels of the FeGe framework, proposed in [1] is not fully realized in the present sample. In order to describe the experimental observations more accurately a new model (III) was introduced. In this model the superstructure is described by an orthohexagonal cell with the dimensions (2*c*, $3a\sqrt{3}$, $a)_h$ as given in [1], but the distribution of Er and Ge-pairs within the hexagonal channels is intermediate between model I (random distribution of Er and Ge_2-pairs along the channels) and model II (perfect long-range order).

Model II is obtained from model I by splitting the Er and Ge1 positions into two positions (see Table 1, left column), which implies the cell enlargement mentioned already above. The positional splitting used in model III, as shown in Table 1, is restricted to the Er1, Er2 and Ge1, Ge2 positions of model II. In order to avoid an unstable

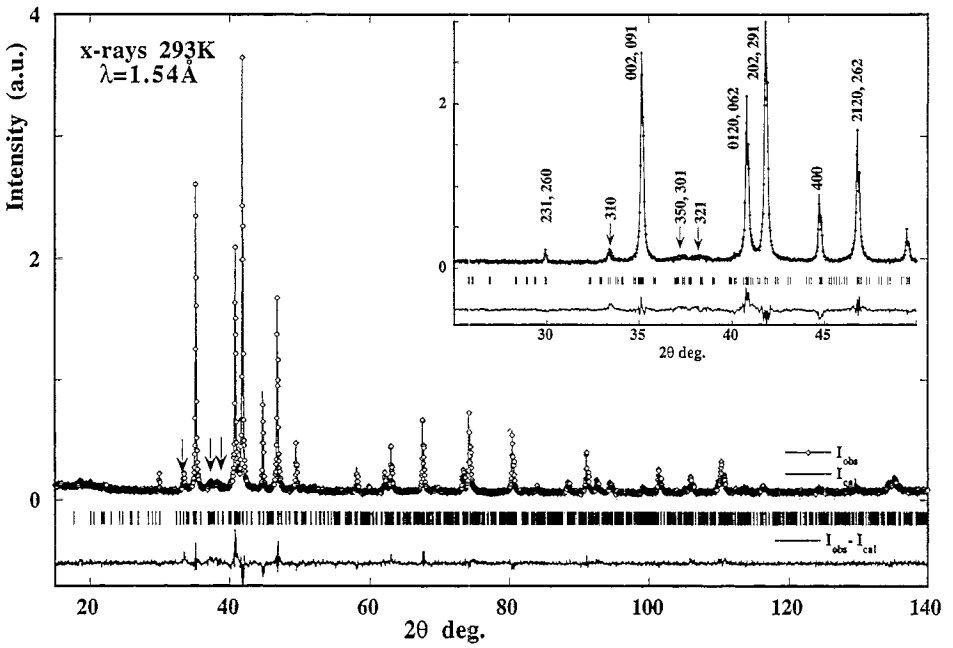

Fig. 1. Observed, calculated and difference X-ray diagram of $ErFe_6Ge_6$ at 293 K calculated for model III (disordered $HoFe_6Sn_6$ structure type, *Immm* (2*c*, $3\sqrt{3}a$, $a)_h$ where $(a, c)_h$ refer to the hexagonal YCo_6Ge_6 cell.

Table 1
Refined atomic parameters from X-ray data of $ErFe_6Ge_6$ for two models: (a) YCo_6Ge_6 (I) left part $(a, c)_h$ *P6/mmm* (b) disordered $HoFe_6Sn_6$ (III), right part $(2c, 3\sqrt{3}a, a)_h$, *Immm*

Atom	Site	x	y	z	Occup.	B_{iso} nm^2	Site	x	y	z	Occup.	B_{iso} nm^2
Er1	1a	0	0	0	0.0801_7	0.026_7	2a	0	0	0	0.080_1	0.026_4
Er2							4h	0	0.1677_4	1/2	0.150_2	0.026_4
Er1*							2b*	1/2	0	0	0.045_1	0.026_4
Er2*							4g*	1/2	y_{Er2}	1/2	0.100_2	0.026_4
Ge1	2e	0	0	0.3076_9	0.183_1	0.14_1	4e	0.3592_6	0	0	0.194_4	0.026_4
Ge2							8n	x_{Ge1}	y_{Er2}	1/2	0.366_6	0.026_4
Ge1*							4e*	0.815_2	0	0	0.046_4	0.026_4
Ge2*							8n*	x_{Ge1*}	y_{Er2}	1/2	0.134_6	0.026_4
Ge3	2c	1/3	2/3	1/2	0.333	0.054_5	2c	0	0.0570_5	1/2	0.25	0.077_4
Ge4							4g	1/2	y_{Ge3}	1/2	0.25	0.077_4
Ge5							4h	0	$2y_{Ge3}$	0	0.25	0.077_4
Ge6							4g	1/2	$2y_{Ge3}$	0	0.25	0.077_4
Ge7							4h	0	$4y_{Ge3}$	0	0.25	0.077_4
Ge8							4g	1/2	$4y_{Ge3}$	0	0.25	0.077_4
Fe1	3g	1/2	0	1/2	0.500	0.030_4	4f	0.2557_9	0	1/2	0.25	0.066_4
Fe2							8k	1/4	1/4	1/4	0.50	0.066_4
Fe3							8n	x_{Fe1}	$4y_{Fe4}$	1/2	0.50	0.066_4
Fe4							16o	x_{Fe1}	0.0830_7	0.251_4	1.00	0.066_4
a, b, c, (nm)		0.510638_8, 0.404995_7					0.80991_1, 2.65293_9, 0.510721_1,					
R_n, R_{wp}, R_{exp}%		9.3, 20.2, 5.7					11.4, 23.2, 6.4					

refinement caused by the low ratio between observations and free parameters and by the pseudosymmetry, we used the following restrictions: (a) the coordinates of atoms were constrained to the same sites as in model I, (b) the occupancies of the split positions (Er1 and Er1*, for example) were constrained to give fully occupied average positions of model II. The results of the refinement are presented in Fig. 1 and Table 1.

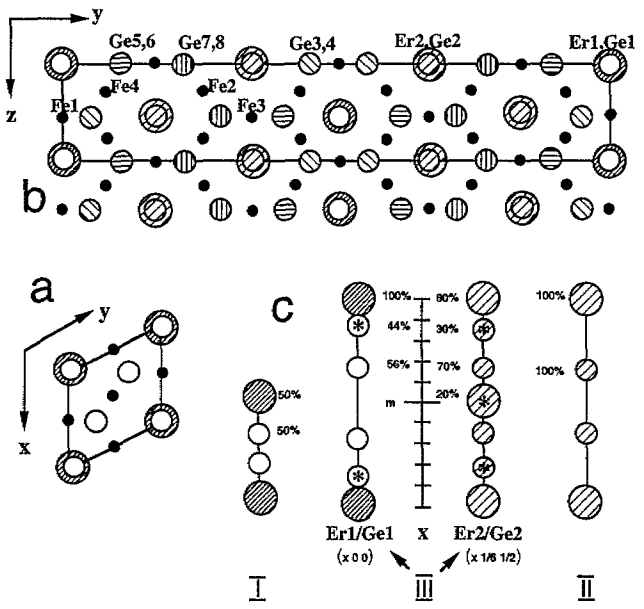

Fig. 2. Atomic arrangement in the $ErFe_6Ge_6$ compound. (a) The YCo_6Ge_6 structure when viewed along [001], model I. (b) The $HoFe_6Ge_6$ structure when viewed along [100], model II. (c) The atomic distribution along the Er/Ge chains of the three different models (I, II, III).

Characteristic features of the diffraction pattern are the broadened shape of the satellites if compared to that of the main reflections, and the presence of diffuse scattering also observed in antiphase domain materials [7,8]. These effects are possibly connected with the relatively small size of the coherently scattering regions in which long-range order of the Er and Ge-atoms prevails compared to the size of the coherently scattering regions of the rigid part of the structure (FeGe-framework). Such a small size of coherently scattering regions may be expected to be due to fluctuations in the atomic density associated with the partly random occupation of Er and Ge atoms of the channel sites, as discussed above. It may also originate from size variations of regions showing identical atomic ordering.

The single crystal of the $ErFe_6Ge_6$ compound used for the magnetic measurements was found to have the cell dimensions $(2c, 2a\sqrt{3}, a)_h$ (*Cmcm*) different from that of the powder sample (*Immm*, $2c$, $3a\sqrt{3}$, $a)_h$. As it will be shown in the next section, the magnetic ordering temperatures do not depend very much on the wave vector value.

4. Magnetic measurements

Results of magnetic measurements are shown in Fig. 3. These measurements were made on the single crystal described above. The measurements were taken at three different temperatures with the magnetic field applied perpendicular and parallel to the longest dimension of the

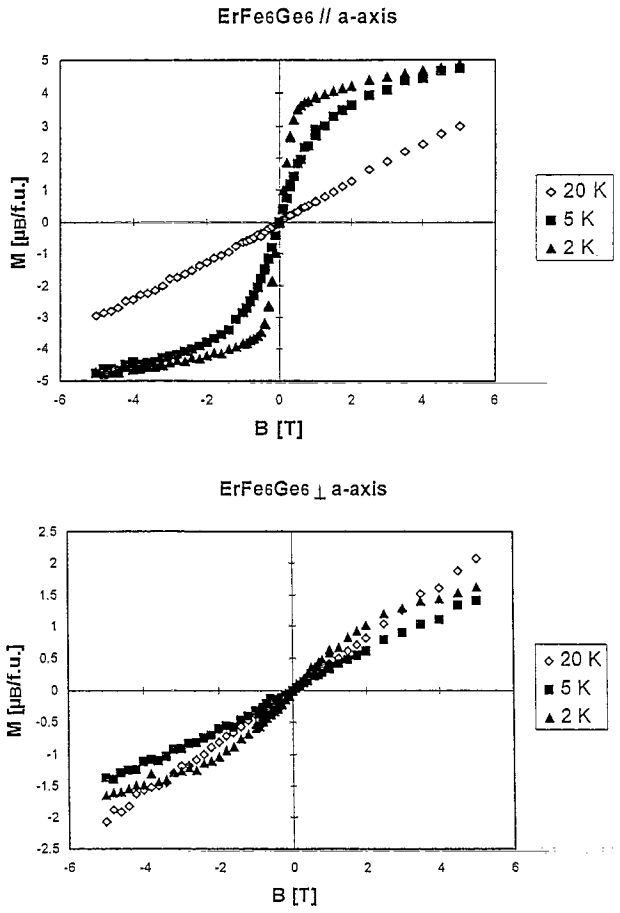

Fig. 3. Field dependence of the magnetisation measured at three temperatures with the field applied parallel (top) and perpendicular (bottom) to the a direction of a single crystal of $ErFe_6Ge_6$. The a direction in the setting used for the structure of the single crystal ($Cmmm$, $2c$, $2\sqrt{3}a$, $a)_h$, where $(a, c)_h$ refer to the YCo_6Ge_6 structure, corresponds to the c direction of the latter structure.

single crystal, the latter corresponding to the crystallographic c_h direction. Because of the rather small dimensions of the single crystal we were not able to align the crystal in a perfect manner with its c_h axis perpendicular and parallel to the field direction.

Comparison of the two sets of data in Fig. 3 shows that there is little difference between the data taken at 20 K. As will be discussed in more detail below, only the Fe sublattice is (antiferromagnetically) ordered at this temperature. The fact that the magnetisation shows only a small difference can be taken as an indication that the Fe sublattice anisotropy is very weak. More pronounced differences between the two sets of data occur at lower temperatures where also the Er sublattice becomes ordered. Apparently the easy magnetisation direction of the Er moments is the c_h direction and there is quite a substantial magnetic anisotropy present. Because of the imperfect alignment of the single crystal, the actual values of the ordered moment are very likely somewhat too low in the upper part of the figure and too high in the lower part of the figure.

5. Neutron diffraction

5.1. High resolution neutron data obtained at 293 K ($\lambda = 1.224$ Å)

The 293 K high resolution neutron patterns in agreement with the X-ray results can be indexed with the orthorhombic cell of the $HoFe_6Sn_6$ lattice (see Fig. 4). Furthermore the pattern entails additional lines of magnetic origin due to the ordering of the Fe sublattice.

5.1.1. Crystal structure

The intensities of the superstructure lines in the neutron diagram are very weak (see inset Fig. 4), as was observed also when using X-rays. However the refinement of these data has provided us with some additional information important for the interpretation of the low temperature data. The refinement of the X-ray data indicates that the Er sites (Er1/Er1* and Er2/Er2*) and the Ge sites (Ge1/Ge1* and Ge2/Ge2*) (see Table 1) may have a different degree of ordering.

High resolution neutron diffraction offers the possibility to release all constrained parameters given in Table 1 and to obtain more accurate occupancy values. The difference Fourier density map obtained from the F_o extracted from the neutron data and F_c based on model II confirmed the existence of positive density at the location of the Er* and Ge* atoms. The refinement shows within 3σ limit no essential deviation of the atomic parameters related to the FeGe framework from their ideal positions. Positional shifts as well as site occupancies of all atoms are summarized in Table 2.

5.1.1.1. Er/Ge disorder

The most important result concerns the atomic distribution of Er/Ge within the [100] channels. The atomic disorder is larger for the Ge than for the Er sites. The resulting atomic distribution within the channels of Er1/Ge1 at (x 0 0) and Er2/Ge2 at (x 1/6 1/2) chains is shown in detail in Fig. 2c and is compared to those of models I and II. Models I and II have a single kind of Er/Ge distribution along the channels. The Er/Ge sites are fully occupied in model II and half occupied in model I. In model III as results from the high resolution neutron data, the $ErFe_6Ge_6$ structure has two distinct kinds of chains. The Er1/Ge1 chain consists of a single Er position (100%) and of two Ge1(56%)/Ge1*(44%) pairs around (1/4 0 0) and (3/4 0 0). The Er2/Ge2 chain consists of two Er positions (Er2(80%)/Er2*(20%)) and two Ge2(70%)/Ge2*(30%) pairs around (1/4 1/6 1/2) (3/4 1/6 1/2).

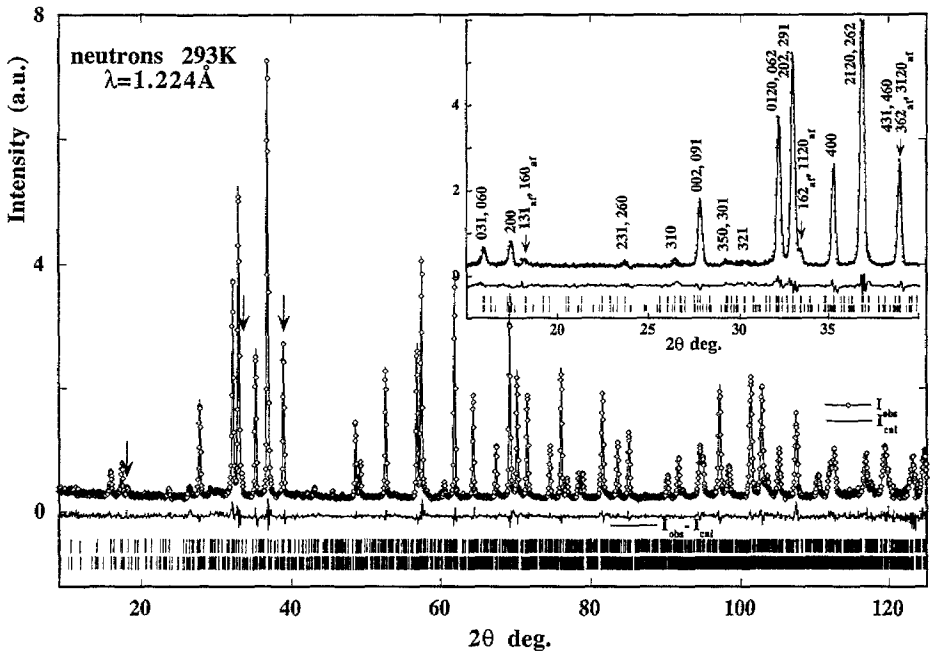

Fig. 4. Observed, calculated and difference high resolution neutron diagram of $ErFe_6Ge_6$ at 293 K with nuclear and antiferromagnetic (Fe) contributions.

The very different Er distribution within the two chains leads to a very different population of the layers at $x=0$ (90% in average) and $x=1/2$ (10% in average). This result is of primary importance in the parametrisation of the low temperature data and the understanding the magnetic ordering of Er-sublattice (see next sections).

Table 2
Refined atomic parameters from high resolution neutron data obtained for $ErFe_6Ge_6$ at 293 K. The refinement is based on the disordered $HoFe_6Sn_6$ (III) model ($2c$, $3\sqrt{3}a$, $a)_h$, *Immm*

Atom	Site	x	y	z	Occup.	B_{iso} nm^2
Er1	2a	0	0	0	0.125	0.18_5
Er2	4h	0	0.1670_9	1/2	0.200_6	0.029_2
Er1*	2b*	1/2	0	0	–	–
Er2*	4g*	1/2	0.1679_6	1/2	0.050_6	0.029_2
Ge1	4e	0.331_4	0	0	0.141_6	0.12_4
Ge2	8n	0.350_1	0.166_1	1/2	0.350_8	0.05_1
Ge1*	4e*	0.858_4	0	0	0.109_6	0.12_4
Ge2*	8n*	0.845_4	y_{Er2}	1/2	0.150_8	0.05_1
Ge3	2c	0	0.0545_6	1/2	0.25	0.01_2
Ge4	4g	1/2	0.0555_8	1/2	0.25	0.08_3
Ge5	4h	0	0.1136_6	0	0.25	0.03_3
Ge6	4g	1/2	0.1112_8	0	0.25	0.11_3
Ge7	4h	0	0.2194_7	0	0.25	0.09_2
Ge8	4g	1/2	0.2229_6	0	0.25	0.05_2
Fe1	4f	0.2524_1	0	1/2	0.25	0.04_4
Fe2	8k	1/4	1/4	1/4	0.50	0.07_2
Fe3	8n	0.250_1	0.3334_5	1/2	0.50	0.10_2
Fe4	16o	0.2516_7	0.0820_2	0.243_2	1.00	0.04_1
μ_x (μ_B/Fe)		1.35(3)				
a, b, c (nm)		0.81008_1, 2.653182_2, 0.510768_1,				
R_n, R_m R_{wp}, R_{exp}%, χ^2		6.0, 16.8, 10.7, 7.2, 2.2				

The very different Er distribution within the two chains leads to a very different population of the layers at $x=0$ (90% in average) and $x=1/2$ (10% in average). This result is of primary importance in the parametrisation of the low temperature data and the understanding the magnetic ordering of Er-sublattice (see next sections).

5.1.2. Antiferromagnetic Fe ordering

The reflections of magnetic origin indicated by arrows in Fig. 4, occur at reciprocal lattice positions that do not obey the I centering reflection condition of the space group *Immm*, leading to the magnetic lattice I_p $\mathbf{q}_1=(010)$. The magnetic ordering associated with the additional reflections involves exclusively the Fe sublattice. The special position of the 8(k) Fe atoms (1/4 1/4 1/4) at the center of symmetry restricts the possible magnetic space groups to those having an anticenter at (0 0 0): $I_pm'm'm'$ (P_Innm, (Sh_{48}^{264})) and I_pmmm' (P_Inmm, (Sh_{59}^{246})) [9,10]. The possible magnetic modes for the four Fe sites are given in Table 3. The refinement has shown that the Fe moments of all sites point to the same direction, along the a axis, and have the same ordered moment value of 1.35(3) μ_B/Fe. This arrangement is invariant under the magnetic space group $I_pm'm'm'$ (Sh_{48}^{264}). The magnetic structure is displayed in Fig. 5. The moments are coupled ferromagnetically within the hexagonal plane but antiferromagnetically in adjacent planes along a. This arrangement is similar to that in the hexagonal modification of FeGe [11].

Noteworthy is the fact that the antiferromagnetic reflections are restricted to the positions of the YCo_6Ge_6 hexagonal lattice with a doubling of the c_h axis. Therefore, one may assume, in a first approximation, that the density modulation of the Er and Ge atoms does essentially not

Table 3
Magnetic modes of the four Fe positions for two possible magnetic space groups compatible with the anticentered lattice I_p and space group *Immm*

	Site	$I_P \frac{2}{m'}\frac{2}{m'}\frac{2}{m'} i'$			$I_P \frac{2}{m'}\frac{2'}{m}\frac{2'}{m} i'$		
	Gen el.	(Sh_{48}^{264})			(Sh_{59}^{246})		
Fe1 $xyz+I_p$	4(f)	x			–		
1. x,0,1/2	e	+					
2. $-x$,0,1/2	2_z	–					
Fe2 $xyz+I_p$	8(k)	x	y	z	x	y	z
1. 1/4,1/4,1/4	e	+	+	+	+	+	+
2. 3/4,3/4,1/4	2_z	–	–	+	+	+	–
3. 3/4,1/4,3/4	2_y	–	+	–	–	+	–
4. 1/4,3/4,3/4	2_x	+	–	–	–	+	+
Fe3 $xyz+I_p$	8(n)	x	y		x	y	
1. x, y, 0	e	+	+		+	+	
2. $-x$, $-y$, 0	2_z	–	–		+	–	
3. $-x$, y, 0	2_y	–	+		–	–	
4. x, $-y$,0	2_x	+	–		–	+	
Fe4 $xyz+I_p$	16(o)	x	y	z	x	y	z
1. x, y, z	e	+	+	+	+	+	+
2. $-x$,$-y$, z	2_z	–	–	+	+	+	–
3. $-x$, y,$-z$	2_y	–	+	–	+	–	+
4. x,$-y$,$-z$	2_x	+	–	–	+	–	–
5. $-x$,$-y$,$-z$	i	–	–	–	–	–	–
6. x, y,$-z$	m_z	+	+	–	–	–	+
7. x,$-y$, z	m_y	+	–	+	–	+	–
8. $-x$, y, z	m_x	–	+	+	–	+	+

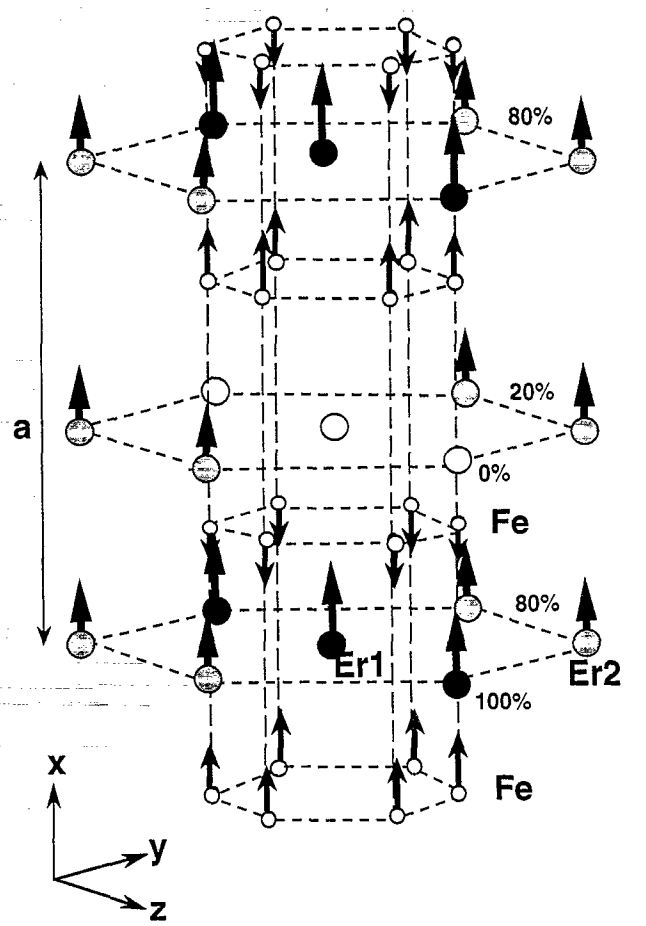

Fig. 5. Schematic representation of the magnetic structure of $ErFe_6Ge_6$. The ferromagnetic Fe sheets are mutually coupled antiferromagnetically. The Er sublattice shows ferromagnetic ordering below 3 K.

affect the Fe–Fe distances and the concomitant magnetic properties which are primarily determined by the honeycomb structure of the FeGe framework.

5.2. Low temperature neutron diffraction

The 4.5 K neutron pattern (Fig. 6, top part) displays the same peak topology as the 293 K high resolution data. This indicates that only the Fe sublattice orders magnetically down to this temperature. The resulting reliability factors are $R_n = 10.1\%$ for nuclear and $R_m = 14.1\%$ for the magnetic structure (Table 4). As expected, the Fe moments values are higher (1.75(4) μ_B/Fe) than at 293 K (1.4(3) μ_B/Fe).

5.2.1. Ferromagnetic ordering of the Er moments ($T = 1.5$ K)

The neutron data obtained at 1.5 K are shown in Fig. 6 (bottom part). When comparing with the 4.5 K neutron data one recognizes that several additional features are present. Besides the magnetic intensities resulting from the antiferromagnetic ordering of the Fe-sublattice substantial magnetic intensity contributions appear at reciprocal lattice positions (indicated by arrows in the bottom part of Fig. 6) of the nuclear structure ($\mathbf{q}_2 = 0$). The only magnetic space group which allows ferromagnetic modes is *Imm'm'* (Sh_{71}^{536}). The best fit ($R_n = 7.5$, $R_{m1} = 7.7$, $R_{m2} = 21.7$) was reached for ferromagnetic ordering of the Er-moments (7.5(2) μ_B/atom) along the a direction (Table 5, Fig. 5). The rather large reliability factor R_{m2} associated with the Er ferromagnetic ordering, apart from overlapping of the magnetic reflections with the overwhelming nuclear reflections, is due to the presence of an anisotropic peak broadening of the ferromagnetic reflections. More detailed numerical analysis is presented in the next section where the difference neutron diagram between the 1.4 K and 4.5 K data is considered.

5.2.2. The difference diagram 1.5 K–4.5 K

The difference neutron diagram obtained by subtracting the 4.5 K data from the 1.5 K data contains only ferromagnetic Er contribution. In Fig. 7 (top part) one observes sharp ferromagnetic main reflections overlapping with a 'wavy background' and a few resolved superstructure lines with $h = 2n+1$ that have a definitely larger halfwidth. Besides, the first (110) superstructure reflection is shifted from its ideal position. The anisotropic peak

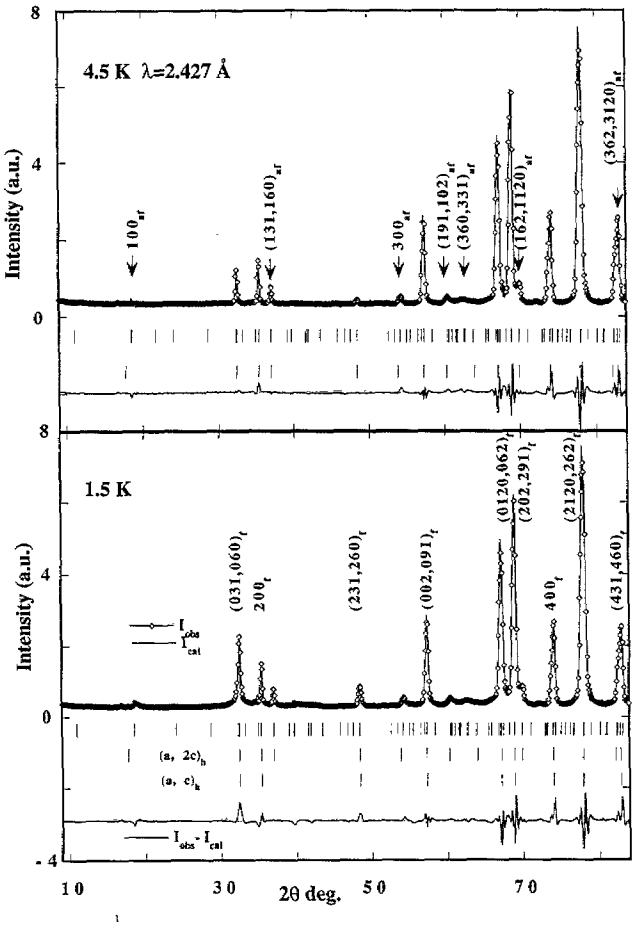

Fig. 6. Observed, calculated and difference neutron diagrams of $ErFe_6Ge_6$ at (a) 4.5 K (top part) with nuclear and antiferromagnetic (Fe) contributions and (b) 1.5 K (bottom part) with nuclear, antiferromagnetic (Fe) and ferromagnetic (Er) contributions. Indexing refers to the ($2c$, $3\sqrt{3}a$, $a)_h$ cell.

broadening prompt us to split the ferromagnetic reflections into two distinct sets. The first set comprises the dominating sharp (main) reflections with $h=2n$ which in addition can be described in the YCo_6Ge_6 hexagonal lattice. The second set corresponds to the very weak superstructure reflections with $h=2n+1$ of the nuclear cell ($2c$, $3\sqrt{3}a$, $a)_h$. These reflections are essentially broadened. This is in fair agreement with the broadening of nuclear satellites originating from the chemical ordering of Er and Ge atoms. This phenomenon is even more pronounced in the magnetic part (superstructure reflections of magnetic origin are broader than nuclear satellites). It indicates that the size of coherently scattered magnetic domains is even smaller than the coherently scattering regions in which long-range order of the Er and Ge-atoms prevails.

Table 4
Refined parameters of $ErFe_6Ge_6$ from neutron data at (a) 4.5 K (ordering of Fe) and (b) 1.5 K (ordering of Fe and Er)

Parameter	4.5 K	1.5 K	1.5 K–4.5 K
μ_{xEr1}, $\mu_{xEr2}(\mu_B)$	–	7.5(2)	8.5(1), 7.22(9)
$\mu_{xFe}(\mu_B)$	1.75(4)	2.0(2)	–
a (nm)	0.8116(1)	0.81169(8)	0.8114(1)
b (nm)	2.65224(4)	2.652960(1)	2.6530(4)
c (nm)	0.510585(7)	0.510550(4)	0.510556(7)
B_{of} (nm^2)	0.010(3)	0.006(3)	
R_n, R_{m1}, R_{m2}, $R_{m2'}$(%)	10.1, 14.1, -, -	7.5, 7.7, 21.7,-	-, -, 7.7,8.1
R_{wp}, R_{exp}(%)	15.7, 0.8	16.8, 0.2	15.7, 0.9

R_n, R_{m1}, R_{m2}, $R_{m2'}$ are the reliability factors for the integrated nuclear, anti- and the two sets ($h=2n$, $h=2n+1$) of ferro-magnetic intensities respectively. The quantity μ is the ordered moment value.

To take the totally observed magnetic intensity into consideration, we used different parameters in the profile fit of the two sets of reflections. Results are given in Table 4. The refinement of the difference diagram revealed that two different Er atoms have slightly different moment values 8.5(1) and 7.22(9) μ_B and are close to the free ion value ($gJ\mu_B=9$ μ_B for Er^{3+}).

5.2.3. Thermal behaviour of the diffuse magnetic scattering

Neutron diffraction patterns recorded at different temperatures in the 1.5–4.5 K interval indicate the presence of diffuse scattering. The enhancement of diffuse scattering in the low 2θ region and in the 30–45° interval can be seen, for example at the 1.5–3.2 K difference diagram shown in the bottom part of Fig. 7. This diffuse scattering is of magnetic origin and indicates the presence of ferromagnetic short range order before long range ferromagnetic order sets in. The effect increases and coexists with long range ferromagnetic order at lower temperatures.

The presence of this short range ordering of the Er moments is most clearly revealed in the magnetic isotherm of a single crystal measured at 5 K. In fact, the ordering of the Er sublattice can be followed rather closely from the results of magnetic measurement shown in the upper part of Fig. 3. The isotherm measured at 15 K is reminiscent of the behaviour of an antiferromagnet which, in the underlying case, is the antiferromagnetically ordered Fe sublattice. In addition to the contribution of the latter there is a smaller contribution due to the paramagnetic Er sublattice leading to some deviation from linear behaviour as the field strength increases. In the isotherm measured at 2 K one recognizes the presence of a strong ferromagnetic contribution which is attributed to ferromagnetic ordering of the Er sublattice. In the isotherm measured at 5 K there is a ferromagnetic contribution which is induced by the applied magnetic field. This contribution can most conveniently be interpreted as resulting from the field-induced growth of regions with prevailing short range ordering, spreading into the whole crystal as the temperature decreases. Most likely the observed low-temperature magnetic ordering behaviour of the Er sublattice (coexistence of long and short range order ferromagnetism) relates to the atomic density fluctuations and the concomitant differences in atomic surrounding which affects the magnetic

Table 5
Part of observed and calculated integrated neutron intensities of $ErFe_6Ge_6$ at 1.5 K

hkl	2θ(°)	I_{cal} nuclear	I_{obs}	I_{cal} AF	I_{obs}	I_{cal} FM	I_{obs}
1 1 0	17.99	279	179			188	365
1 5 0	31.72	168	184			498	507
0 3 1	31.86	1808	2009			2443	2489
0 6 0	31.87	668	743			2443	2489
1 2 1	34.35	178	77			446	364
2 0 0	34.79	2723	3208				
1 3 1	36.42			325	311		
1 6 0	36.42			325	311		
1 4 1	39.16	116	24			363	166
1 7 0	41.39	112	40			330	259
2 6 0	47.89	212	338			490	456
2 3 1	47.89	216	344				
3 1 0	53.59	357	926				
1 8 1	54.94	46	22			212	199
0 0 2	56.77	3663	3669			765	739
0 9 1	56.77	7191	7206			765	739
1 9 1	59.78			108	128		
1 0 2	59.78			105	125		
1 1 2	60.06	88	111			177	222
3 5 0	60.45	276	304			40	59
3 0 1	61.00	70	140				
3 2 1	62.09	418	609			45	88
3 6 0	63.44			27	36		
3 3 1	63.44			27	36		
1 11 0	63.32	12	16			167	260
1 10 1	64.93	125	136			150	193
3 4 1	65.30	303	387			51	67
1 5 2	66.50	78	78			150	195
0 6 2	66.58	17291	17072			562	729
0 12 0	66.58	7838	7738			562	729
3 7 0	66.88	185	207			52	70
0 11 1	67.64	905	939				
2 0 2	68.32	11246	11480			383	446
2 9 1	68.33	22542	23015	469	446	383	446
1 12 0	69.35			643	633		
1 6 2	69.35			643	633		
1 7 2	72.64	75	45			125	108
4 0 0	73.44	12998	13825				
1 13 0	75.63	5	6			113	146
2 12 0	77.37	18016	17783			323	461
2 6 2	77.37	33017	32590			323	462
3 8 1	77.47	301	299			59	85
3 9 1	81.62			25	28		
3 0 2	81.62			25	27		
3 1 2	81.85	294	309	19	24	51	56
4 3 1	82.28	10290	10959			54	58
4 6 0	82.28	4733	5041			54	58

The left, middle and right parts comprise nuclear, AF and FM (Fe- and Er-sublattices) intensities. Indexing refers to the $(2c, 3\sqrt{3}a, a)_h$ cell.

coupling between the Er moments. It is expected that the ratio of these types of ordering is sample and temperature dependent.

5.2.4. Thermal behaviour of the magnetic intensities

The thermal variation of the integrated intensities of the antiferromagnetic reflections as represented by the (131) (160) reflections in Fig. 8 shows virtually no variation in the temperature interval 1.5 K–4.5 K. By contrast, the intensity of the ferromagnetic (031) (060) and (231) (260) reflections varies strongly in the low-temperature regime. From these data one may derive that the ferromagnetic ordering of the Er moments takes place at 3 K. The same behaviour is found for the (110) superstructure line. This ordering temperature as well as the refined Er moment value are in fair agreement with the results of Wang et al. [3].

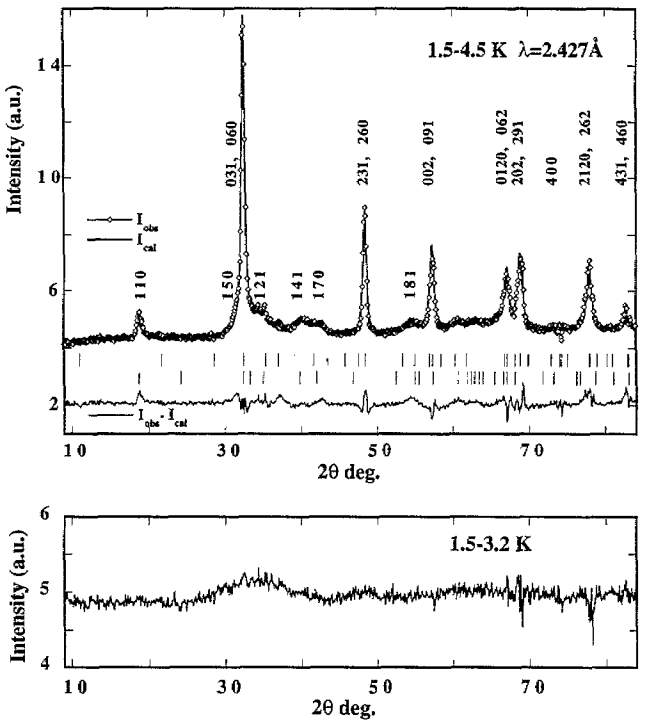

Fig. 7. Difference neutron diagram obtained by subtraction of the 4.5 K data comprising only nuclear and Fe ferromagnetic contribution from the 1.5 K data. Indexing refers to two sets of ferromagnetic reflections of Er-sublattice (top part).

Difference neutron diagram obtained by substraction of the 3.2 K data from the 1.5 K data showing the existence of short range order effects (bottom part).

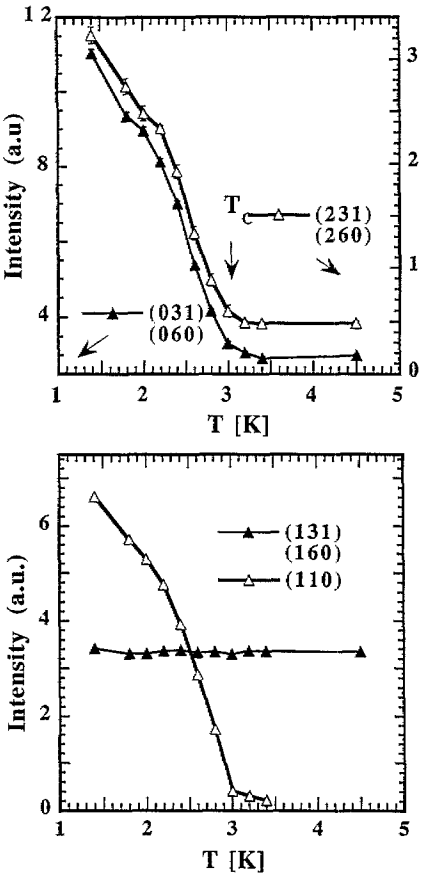

Fig. 8. Thermal variation of the integrated intensity of the ferromagnetic + nuclear (231)(260) and (031)(060) lines, the (110) satellite and the antiferromagnetic (131)(160) lines.

6. Concluding remarks

The crystal structure and magnetic ordering of $ErFe_6Ge_6$ were studied by means of X-ray diffraction, neutron powder diffraction and magnetic measurements on single crystals. The refinement suggests that the crystal structure (model III) is intermediate between perfectly ordered structure ($HoFe_6Sn_6$ structure type, model II) and absolutely disordered phase (YCo_6Ge_6 structure type, model I). The results of the refinements of the X-ray diffraction and high resolution neutron powder data at 293 K are in fair agreement as regards the positional parameters and the majority of the occupational parameters of the atoms. The largest discrepancy is observed in the relative population of the Er1/Er1* and Ge1/Ge1* sites. As Er and Ge atoms are strong scatterers for neutrons (Ge is much weaker for X-rays) we consider neutron data refinement as the more reliable one.

The 293 K and the 4.5 K neutron data show that the antiferromagnetic reflections can be attributed to the ordering of the Fe-moments. The collinear antiferromagnetic magnetic structure is composed of ferromagnetic Fe-sheets coupled antiferromagnetically along the *a* axis, and it is similar to that observed in the binary FeGe parent phase (CoSn-B35 type). The ferromagnetic ordering at 3 K is exclusively associated with the ordering of Er-moments along the a- axis. Both the single crystal and powder data indicate the presence of short range order magnetic effects. Upon lowering the temperature, these effects coexist and appear before the onset of long range ferromagnetic order.

The two sublattices order independently. The fact that the ferromagnetic and the antiferromagnetic ordering types are described by two different magnetic space groups indicates the presence of two order parameters which explains the independent behaviour of the Fe and Er sublattices. Alternatively it could be said that the common magnetic space group ($P2m'm'$) is the intersection of the ferromagnetic ($Imm'm'$) with the antiferromagnetic ($I_Pm'm'm'$) space group. The *I*-centering becomes I_P when the Fe-moments become ordered, and gets lost together with the center of symmetry when the ordering of the Er moments sets in.

The ferromagnetic behaviour of the R sublattice in $ErFe_6Ge_6$, if compared to the corresponding $ErMn_6Ge_6$ compound [12] is presumably a consequence of the modified R–R interaction along the hexagonal axis at distance $c_h/2$ which, in turn, is a consequence of the introduction of different R–R distances associated with the

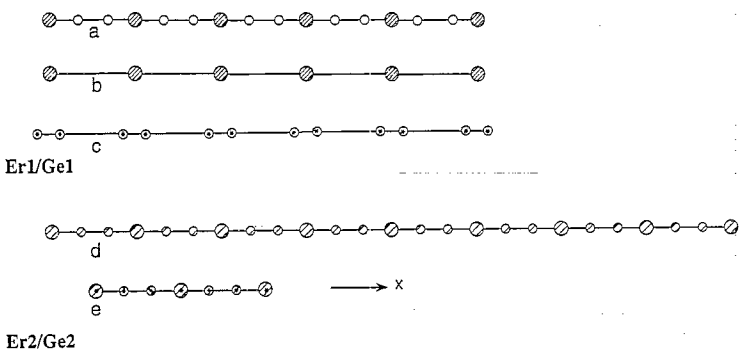

Fig. 9. Schematic representation of segments of the Er1/Ge1 (a, b, c) and Er2/Ge2 (d, e) chains showing preferable places of stacking faults and different length of regions with long range order of Er and Ge atoms in the channels along the [100] direction. The ratio of the length of different segments corresponds to refined occupancy of star and nonstar positions (see Section 6 for details).

density modulations observed for the R and the Ge site along the c_h axis.

The broadening of the nuclear superstructure lines relative to the main reflections indicates that the coherently scattering regions, characterised by similar long range order of the Er and Ge-atoms within them, are of relatively smaller size compared to the size of the coherently scattering regions of the FeGe-framework. The ferromagnetic superstructure reflections are even broader than the nuclear satellites, meaning that the coherently scattering regions of ferromagnetic Er-moments are even smaller. These observations can be explained qualitatively by following pictures of the actual structure of $ErFe_6Ge_6$ (Fig. 9). The structural model III based on the refinement of our neutron powder data is the average over all diffracting crystallites and microdomains. Disorder in Er1/Ge1 and Er2/Ge2 chains implies occupation of either nonstar (Er, Ge) or star (Er*, Ge*) positions and means averaging over regions of the crystal where segments like those presented in Fig. 9 are realized. For obtaining the average population of the Er1/Ge1 chain as presented in Table 3 three different segments in a ratio 1:1:1 are required (Fig. 9 a,b,c). The Er2/Ge2 chain consists of two segments (Fig. 9 d,e) in a ratio 7.5:2.5. The change of the segments can lead to a stacking fault or an antiphase boundary. It does not affect the FeGe-framework, but can reduce the coherently scattering region of the superstructure lattice. In the diffraction pattern this is manifested by broadening of the superstructure lines comparing to the main reflections. The segment *c* of the Er1/Ge1 chain contains only Ge1* atoms. Hence, coherent regions when the Er is atomically ordered can be even smaller than coherent regions composed of atomically ordered Er and Ge. When the Er moments order ferromagnetically at low temperatures this effect will manifest itself by a broader shape of the magnetic superstructure lines.

As the magnetic ordering of the Er moments depends sensitively on density distribution it is expected that the ratio of the long range and short range ordering will depend on the sample preparation. Neutron measurements on various other RFe_6Ge_6 compounds are in progress.

Acknowledgments

This work is financially supported by the Swiss National Foundation, Bern.

References

[1] G. Venturini, R. Welter and B. Malaman, J. Alloys and Comp., 185 (1992) 99.
[2] B. Chafik El Idrissi, G. Venturini and B. Malaman, Mat. Res. Bull., 26 (1991) 1331.
[3] Y.B. Wang, D. Wiarda and D.H. Ryan, IEEE Trans. Magnet., 30 (1994) 4951.
[4] D.H. Ryan and J.M. Cadogan, J. Appl. Phys., 79 (8) (1996) 6004.
[5] J. Rodriguez-Carvajal, Physica B 192 (1993) 55.
[6] S.R. Hall, G.S.D. King and J.M. Stewart (eds.), XTAL3.4 User's Manual, University of Western Australia, Lamb, Perth, 1995.
[7] B.E. Warren, X-ray Diffraction, Addison-Wesley, Reading, MA, 1969; reprinted Dover, New York, 1990.
[8] M.A. Krivoglaz, Diffuse Scattering of X-rays and Neutrons by Fluctuations, Springer-Verlag Berlin, Heidelberg, 1996.
[9] W. Opechowski and R. Guccione a) in G.T. Rado and H. Suhl (eds.), Magnetism IIA, Academic Press, London, 1965 Ch 3, p. 105. b) Ann.Phys. 2 (1977) 121.
[10] V.A. Koptzik, Shubnikov Groups, Moscow University, print 1966.
[11] J.B. Forsyth, C. Wilkinson and P. Gardner, J. Phys. F: Metal Phys., 8 (1978) N10 2195.
[12] P. Schobinger-Papamantellos, G. André, J.J. Rodríguez-Carvajal and K.H.J. Buschow, J. Alloys Comp., 219 (1995) 176.